CrossMark

Design and Evaluation of an Experimental Technique for Mechanical and Fatigue Testing of Sub-Sized Samples

I. V. Lomakin[1] · A. R. Arutyunyan[1] · R. R. Valiev[1,2] · F. A. Gadzhiev[1] · M. Yu. Murashkin[1,2]

Abstract

Some recently developed processing techniques allow fabrication of small specimens. The fatigue behavior of these small samples cannot be characterised according to the existing standards due to size limitations. The main objective of the present work is to develop an original technique for both mechanical and fatigue testing of sub-sized specimens produced by a high pressure torsion (HPT) method. The fatigue behavior of the sub-sized Ti-6Al-4 V samples, made from HPT-processed disks, is compared with that of the standard samples prepared according to the ASTM standards. Finite element method (FEM) analysis of the stress distribution under applied static load, for both sub-sized specimens and grips designed for their testing, is performed. Good agreement between the outcomes of tensile testing of the standard ASTM samples and sub-sized samples is observed. Fatigue data, represented by Wöhler curves for both types of samples, showed significant divergence of high cycle fatigue properties caused by incompliance of specimen geometries and surface/defect size ratio. The obtained results can be used to scale up the fatigue behavior from sub-sized specimens to the standard ones, as well as to predict the fatigue behavior of the bulk nanostructured metals and alloys produced by HPT.

Introduction

It has often been a challenging task to study the mechanical behavior of materials which can be processed in small quantity. Examples include nanostructured materials produced by inert gas condensation, or severe plastic deformation (SPD) techniques such as high pressure torsion (HPT), where small disks with a diameter up to 20 mm and a thickness of up to 2 mm can be produced. In this case, sub-size specimens (i.e. specimens with smaller dimensions compared to those provided in the standards) have to be tested. Sub-size dog-bone samples of ultra-fine-grained (UFG) Al, nano-Cu, and nano-Ni made by inert-gas condensation and compaction, with 3 mm overall length and cross section gauge of 200 μm × 200 μm,

were tested by uniaxial tension in [1] to study deformation mechanisms and tensile strength. Other successful examples include a series of papers related to fatigue testing of sub-size steel specimens subjected to irradiation [2–5]. The sub-sized specimen were used due to the limited volume of material that can be installed in a reactor. Different specimen geometries (hourglass, dog-bone, or Charpy), as well as different modified experimental techniques, were used [2–5]. These works showed that the mechanical properties, as well as microstructure evolution and mechanisms operating during plastic deformation, can be investigated using sub-size specimens.

Over the last two decades there has been intensive research activity on bulk nanostructured (NS) and UFG materials produced by SPD [6, 7]. It was found that grain refinement leads to significant changes in the basic properties of widely used metals such as copper [8, 9], titanium [10], aluminum [11, 12], nickel [13], and their alloys. Besides a notable increase in strength, severely deformed materials can demonstrate improved functional properties such as electrical conductivity [14], wear [15], and corrosion resistance [16, 17]. A great number of processing techniques to manufacture NS and UFG materials have been developed [18–25], of which equal channel angular pressing (ECAP) [26] and HPT [18] are key techniques among them.

✉ I. V. Lomakin

1 Saint Petersburg State University, Saint Petersburg 199034, Russia

2 Institute for Physics of Advanced Materials, Ufa State Aviation Technical University, Ufa 450000, Russia

Recent results showed that a finer microstructure can be achieved using HPT processing with grain size less than 200 nm [6]. It was shown that such a microstructure provides a high yield limit according to the Hall-Patch law as a result of grain refinement and an increase of dislocation density. It is reasonable to suggest that the UFG materials with enhanced mechanical properties can demonstrate improved fatigue behavior with higher endurance limits. Verification of this statement for a wide range of the HPT processed materials could be the impulse to develop this technique, and for commercialisation of these materials in such important industrial sectors as aerospace, electrical engineering, and medical technologies. At the same time, the fatigue experiments on HPT processed disks have been carried out to date due to the small disk sizes [27, 28]. To enable testing of sub-sized specimens made from HPT processed disks, additional suitable equipment for fatigue experiments, with fine tolerances, should be developed to achieve reliable results. Just a few examples of successful fatigue testing of HPT processed disks can be found in the literature. Miniaturised beam-shaped fatigue samples with dimensions of $4 \times 1 \times 0.6$ mm, machined from UFG medium carbon steel, were cyclically tested using the four-point-bending technique in [29]. The effect of HPT-processing on endurance limit and fatigue mechanisms was studied. Another work focused on the fatigue behavior of an UFG Al-Mg-Si alloy [30]. Sub-sized hourglass specimens for fatigue testing, and dog-bone specimen geometries with total specimen length of 16 mm, were used. The Wöhler curves and tensile properties, for both CG and UFG alloys, were obtained by testing these specimens. It was shown that HPT processing significantly affects both tensile and fatigue behavior. The classical stages of fatigue crack growth were identified on fatigue fracture surfaces of both CG and UFG Al 6061 alloys. These results showed the significant potential of SPD processing to produce materials with enhanced fatigue performance. It was also shown that cycling tests of sub-sized specimens can be performed.

Despite the specimen geometry being provided in these publications, they were lacking in a description of additional facilities produced and used for experiments. The exception is work [5], where significant attention was paid to experimental technique in terms of sample positioning in the grips. Nevertheless, during experimental design, one should also take into account such important aspects as stress concentration areas in both sample and grips, as it can lead to sample fracture in undesirable regions and to incorrect results. No clear data on the effect of sample geometry in fatigue properties can be found in the literature. The aim of this study was to design and develop a unified experimental technique for mechanical and fatigue testing with respect to compare obtained cyclic tests and fracture features over mini-sized samples with standard ones. Proposed

experimental technique is planned to be used for carrying out an experimental fatigue data for a wide range of widely studying metals and alloys processed by HPT with reasonable comparison and tendencies definitions.

Material and Techniques

Material

A CG titanium Ti-6Al-4 V (Grade 5) alloy was chosen for this study. Due to its strong mechanical properties, this alloy is widely used for large aircraft parts, engines, high internal pressure and temperature cylinders, as well as in medicine for dental implants, in particular. In aircraft manufacturing this alloy is widely used for the production of engine turbine blades. It is obvious that for safe exploitation such elements should work effectively in a cyclic load. Recent research on an ECAP processed alloy showed that grain refinement leads to gains in fatigue strength [19]. It suggests the possibility for improvement of mechanical and fatigue properties through grain refinement via HPT processing. A CG alloy was chosen for this study to verify the proposed experimental technique. Furthermore, fatigue results obtained for CG sub-sized specimens will be used for determination of the influence of HPT processing on fatigue behavior of Ti-6Al-4 V alloy.

Samples for mechanical and fatigue testing were cut from a hot rolled 15 mm diameter rod using a spark erosion machine. All samples were prepared so that their tensile axis was along the rolling direction. An $\alpha + \beta$ two phase microstructure, represented by elongated α-grains with β particles in the grain boundaries, was revealed in the alloy by scanning electron microscopy (SEM) and analysis of X-ray diffraction (XRD) patterns (Fig. 1).

The Tensile and Fatigue Specimens

In order to reveal the difference between the proposed experimental technique and a standard one, two sample geometries were designed: sub-sized samples (SS-type) and standard samples (ST-type). The schematic drawings for both geometries are presented in Fig. 2. In the SS-type sample design, the following factors were taken into account:

– **Specimen clamping.** The Specimen geometry was designed for under-the-shoulder load application. This approach allows minimising the shoulders of a specimen in favor of the gauge length, which is important for small specimens. Besides, this principle is currently a trend in mechanical testing of the HPT processed disks, allowing for the possibility of comparison.

– **Versatility.** The main clamping principle of the sample implies that its shoulders are leaning on the support grip but are not squeezed as in the standard experimental
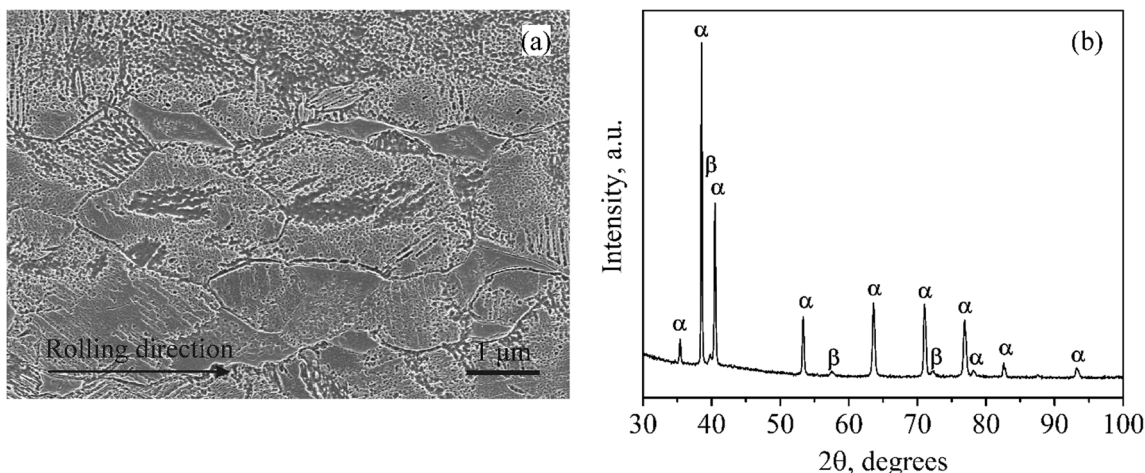
Fig. 1 SEM images (**a**) and XRD patterns (**b**) of the Ti-6Al-4 V alloy with α + β two-phase structure

techniques. Such a testing technique required the production of additional original equipment. One can conclude that the design of this equipment should be done in such a way that it can be integrated into standard experimental testing machines. It is also important that the same equipment can be used for both tensile and fatigue experiments.

– **Compression mode suitability.** As HPT processed material is a flat disk, production of a cylindrical threaded specimen with representable cross section area became impossible. However, specimen and equipment geometries design should be done in such a way that allows compression deformation. Our approach allows for fatigue testing with different R-ratios.

– **HPT processing microstructural features.** It is known that HPT processing not only refines the grain structure, but creates a circular grain texture following on from the rotational nature of the deformation. A grain circular elongation results in anisotropy of mechanical properties. Considering this fact, our design can be used to avoid

undesirable stress concentrations that can be triggered by this anisotropy and lead to premature specimen fracture or stress field distortion during deformation.

The sub-sized specimen geometry for mechanical and fatigue testing, designed according to the specific features mentioned above, is presented in Fig. 2(a). The dimensions were chosen so two samples can be machined from one HPT processed 20 mm diameter disk. The final thickness of the designed samples was 1 mm. To avoid friction, the specimens were designed for under-the-shoulder gripping. Such an approach avoids the production of sophisticated equipment containing many small parts moving with respect to each other. In order to exclude significant extrusion of shoulders through the clamping system, the angle of the supporting shoulders was equal to 125°. This choice was also motivated by a desire to minimise the stress factor at the inevitable stress concentration nodes of the testing grip recess. In addition, the specimen
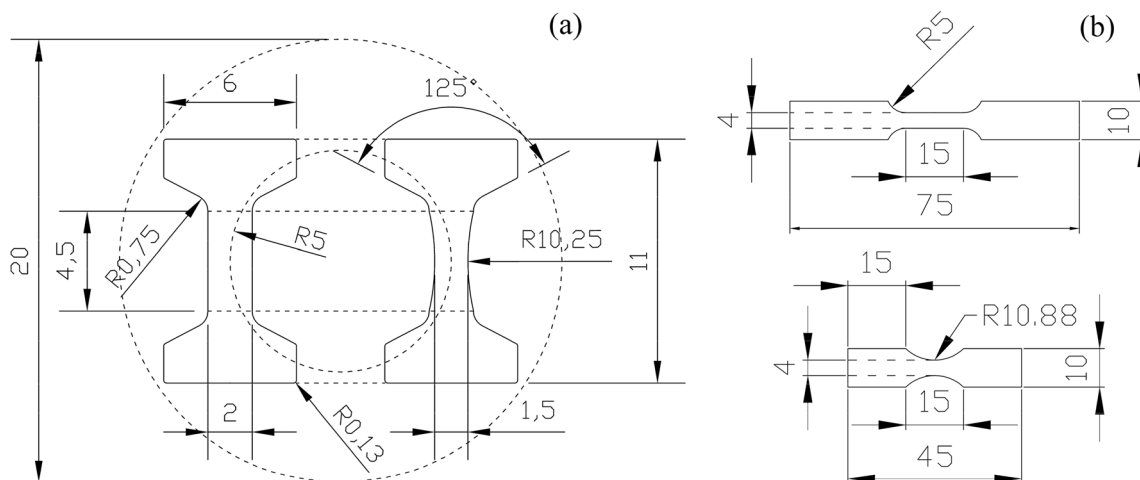

Fig. 2 SS-type (**a**) and ST-type (**b**) specimen geometries for mechanical and fatigue testing. Dimensions are given in millimeters

inner shoulder directions are not collinear to the HPT structure texture if using such a layout. To provide a compression mode during fatigue testing, the top edges of the shoulders were designed to be placed exactly in the grip recess, which had the same shape without any clearance. A 6 mm shoulder width and 2 mm basic gauge width allows a 0.75 mm radius fillet between shoulder and gauge to minimise stress concentration in this part of the sample. This factor is important for fatigue testing of a specimen. A gauge length of 4.5 mm for both tensile and fatigue specimens was chosen. A gauge width of 2 mm for tensile specimens results in a width to length ratio of 4:9 and gauge cross section equal to 2 mm^2. For fatigue specimens, an hourglass shape with 10.25 mm radius and narrowest cross section of 1.5 mm was used. These dimension result in a 1.5 mm^2 cross section with thickness to width ratio of 2:3. The dimensions of specimens had a very high accuracy. An ARTA 123 Pro electric discharge cutting machine was used to accurately machine the specimens. High tolerance was guaranteed by considering the pre-measured (175 μm) gap. It allows achievement of a ± 5 μm tolerance over all dimensions. After sample production, they were polished using a 50 nm final Buehler Master Prep polishing suspension. A Buehler EcoMet 250 polishing machine was used for the plane surfaces of specimens. A Proxxon Micromot 50/E engraving set equipped by felt disks was used during polishing of specimen edges.

To study the effect of specimen shape on the mechanical and fatigue properties of the Ti-6Al-4 V alloy, special grips for clamping specimens by friction were designed (Fig. 2(b)). For tensile testing, dog-bone specimens with gauge length x width x thickness dimensions of $15 \times 4 \times 1$ mm, were used. Hourglass fatigue specimens with 10.88 mm gauge radius and the narrowest cross section of 4 mm^2 were used.

Original Specimen Mechanical Test Cradle

The original cradle designed for fatigue testing was produced by a spark erosion machine. An expanded view drawing of the cradle with its parts is presented in Fig. 3. The specimen mounting process is the following. Base plates A are placed in both necklines of the mounting frame and fixed there by M3x5 socket set screws. The shoulders are then adjusted in grips B and installed on the base plates A. Clamping pins D are placed in the recess of grips B and are covered by clamping plate C. After that, M5x15 screws are threaded through A, B, and C parts 5 mm diameter orifices and fixed by nuts from the other side of the base plate A. A double nutted fixing was used to avoid unwinding during high cycle fatigue testing. After the whole system is ready, it can be placed in standard cyclic and tensile testing machines using suitable friction grips. The mounting frame is removed by unscrewing holding socket set screws releasing the specimen. A special shape for base plate (part A) is designed to avoid
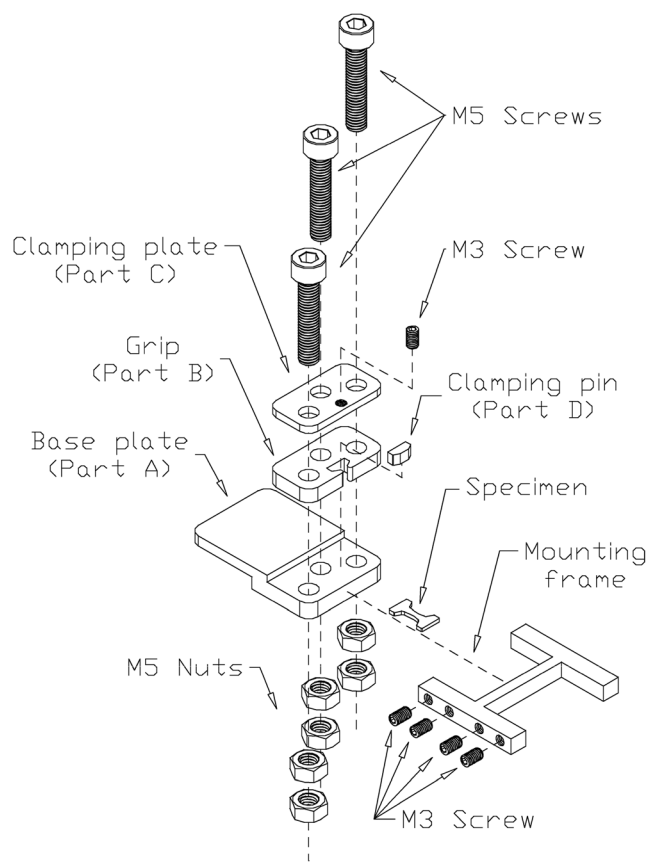
Fig. 3 Zoomed view drawing of the cradle used for mechanical and fatigue testing of SS-type specimens

misalignment of the sample axis and tensile axis of the fatigue testing machine grips. Step notches made on the opposite edges of the plate were designed to align 1 mm thick sample axis with the testing machine axis and exclude any bending of the sample during mechanical testing. Careful adjustment of the testing machines before experiments guaranteed coaxiality of the upper and lower grips.

Stainless steel was used for parts A, C, and the mounting frame. Meanwhile, high-strength high-speed steel was used to produce parts B and D. This steel billet was subjected to the following thermal treatment: annealing at 800 °C for 30 min, further annealing at 1220 °C for 1 h followed by oil quenching, and subsequent triple aging at 560 °C for 1 h followed by slow cooling in the furnace. After such thermal treatment, this alloy is characterised by a high elastic modulus (230 GPa) and yield limit (over 3.4 GPa in bending mode) and outstanding fatigue behavior without plastic deformation. Because of these characteristics, this material was chosen for grip part production to provide a significant lifetime increase for this part of the system under cyclic loading conditions.

It is obvious to conclude that such a grip layout (Fig. 3) leads to the appearance of stress concentration in both grips and specimen fillet between the shoulder and gauge section. Despite the fact that the grip material is significantly stronger

than most of the commonly studied SPD processed materials (copper, aluminum, and titanium alloys), these stress concentrators can cause a fracture in these regions during low cyclic fatigue testing under high stress conditions, or at a high cyclic testing under low stress conditions. To illustrate stress concentration nodes and estimate its influence on the deformation process, a finite element method (FEM) analysis of the "grip – specimen" system was performed. A 99448 SOLID187 3D element with 10 nodes was used for meshing. The solution was found using one-eighth of the whole task using geometry symmetry. A zero displacement was applied on the orifice inner upper planes, while structural loading was achieved by applying 40 μm tension displacement on the specimen's narrowest cross section plane. A contact surface-to-surface pair with friction coefficient value of 0.5 was created. The results presented in Fig. 4(a) show that the stress concentration nodes appeared on the grip's rounded corners and specimen's fillet between the shoulder and hourglass gauge. Even though the stress value in these nodes doesn't exceed the yield limit for both corresponding materials, a relatively high value stress field during cyclic loading can initiate a fatigue crack growth in these regions of the part. This statement was confirmed during first tests over SS-type specimens using manufactured equipment. A brittle failure in the FEM predicted nodes was observed (Fig. 4(b, c)). Failure of Part B (Fig. 4(b)) took place after subsequent operation for 18,491 cycles with 1000 MPa stress, 28,650 cycles with 900 MPa stress, 47,964 cycles with 800 MPa stress, and 72,994 cycles with 700 MPa stress values applied to the specimen. In total, a grip endurance was characterised by operation for 168,099 cycles with stresses

from 1000 to 700 MPa applied to the specimen. After grip failure it was replaced, and the new one was used to complete the Wohler curve with 10^7 cycles fatigue limit. In general three grips were used to obtain one S-N curve in the stress range of 300–1000 MPa for a total of $2 \sim 3 \times 10^7$ cycles.

In contrast to the grips, the stress concentration problem of specimen shoulder fracture during cyclic testing was solved by applying compression force to the specimen head plane surface. This was achieved by adding clamping pin D (Fig. 3) made from the same material as the grips. A compression stress field was induced in the specimen shoulder by tightening an M3 clamping screw, which leads to stress field distortion in this region and, as a result, the stress concentration value decrease. After addition of the clamping pin in the cradle system, a cyclic fracture appears only in the narrowest cross section of the specimen (Fig. 4(d)). This equipment was used to carry out mechanical and fatigue testing of sub-sized specimens.

Other Techniques

An XRD study was carried out using Bruker "D8 Discovery" high definition X-Ray diffractometer with CuKα radiation. The 2θ Bragg angle varied from 30° to 80° and a scan rate of 5°/min was used. The tensile tests were carried out using a Shimadzu AGX-50 Plus universal mechanical testing machine with strain rate of 5×10^{-4} s^{-1}. The desktop servo-hydraulic fatigue test machine Si-Plan SH-B was used for cyclic testing. The loading frequency during experiments was equal to 30 Hz for all specimens. Experiments on small

Fig. 4 A von Mises stress FEM contact pair solution of the grip/specimen system (a) with related fractured grip (b) and mini-sized specimen (c). (d) – fractured mini-sized specimen after clamping pin D addition
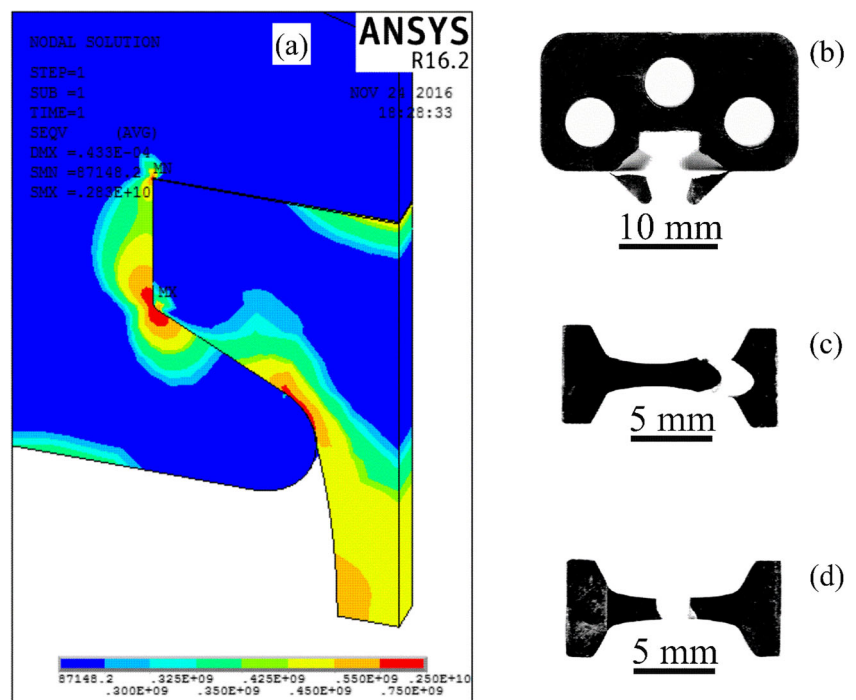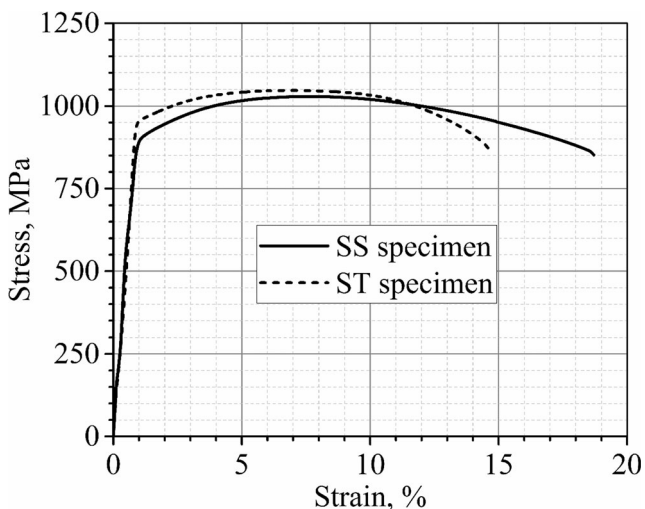
specimens were carried out using in-house designed original additional equipment integrated into the fatigue test machine. The fatigue fracture surfaces were studied with SEM using the Zeiss AURIGA Laser operating at an accelerating voltage of 15 kV.

Results

Mechanical Properties

Figure 5 illustrates a comparison of tensile stress-strain curves for SS and ST specimens. One can see that the mechanical properties of ST specimens are in a good agreement with data from the literature for this alloy. Nevertheless, a significant difference in elongation to failure (δ) exists. Thus, the δ_5 value for SS specimens is $14.5 \pm 0.4\%$, while the same parameter for ST specimens was $19 \pm 0.8\%$. Such a discrepancy can be explained by the fact that SS specimens had a smaller gauge length and surface area than the ST ones. This leads to a lower concentration of the structural and surface defects with equal microstructural features such as grain size, grain shape, and dislocation density. In fact, the carriers of microstructural plastic deformation in the gauge section are represented by a smaller amount in the case of SS specimens, which leads to higher plastic strain resistance ability. However, stress parameters such as the yield limit (σ_y) and ultimate tensile stress (σ_{uts}) were equal for SS and ST specimens. ST specimen stress-strain curves were characterised by average σ_y and σ_{uts} values equal to 1000 MPa and 1085 MPa respectively, while SS samples for the same parameters had values of 950 MPa and 1040 MPa.

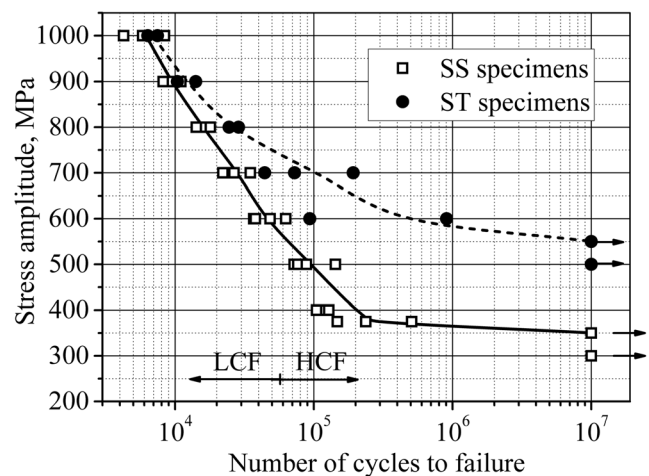Despite different values of elongation to failure being demonstrated by SS and ST specimens, the fatigue curves with constant stress amplitude for both specimen types can be achieved using the same stress values.

Fatigue Properties

The high cycle fatigue (HCF) experiments with constant stress amplitude in tension, with the coefficient of cycle asymmetry $R = 0$, were conducted on SS and ST specimens made of Ti-6Al-4 V alloy. The fatigue experimental results, represented by the S-N curves, are shown in Fig. 6. One can see that fatigue tests on SS-type specimens can be used to plot a relevant Wöhler curve with good statistical dispersion. In the low cycle fatigue (LCF) region the S-N curves for SS and ST specimens are close to each other. Thus, for $N = 10^4$ cycles the stress is the same and is equal to 900 MPa. A significant difference between the fatigue curves for the two specimen types was observed in the HCF region. For $N = 10^6$ cycles the stresses are equal to 365 MPa and 585 MPa for SS and ST specimens, respectively. For stress equal to 600 MPa the number of cycles to fracture for ST specimens is approximately equal to 3.5×10^5, and for SS ones it is 5×10^4, i.e. with number of cycles seven times less.

It should be noted that the value of stress amplitude at number of cycles to failure above 2×10^5 (corresponding to the HCF region), for ST specimens, is higher by a factor of 1.55–1.60 for hot rolled Ti-6Al-4 V, compared to that for the SS specimens. Obviously, this factor can depends on the processing parameters, thermal treatments, microstructural features and, more importantly, may vary significantly for different materials. Here further studies are necessary to more carefully clarify this issue.

As a result of the experiments performed, the fatigue limit based on 10^7 cycles was estimated. It is equal to 350 MPa for

Fig. 5 Stress-strain diagrams for sub-sized (solid line) and standard (dashed line) specimens of CG Ti-6Al-4 V alloy

Fig. 6 Fatigue curves for mini-sized (solid line) and standard (dashed line) specimens of CG Ti-6Al-4 V alloy

SS-type specimens and 550 MPa for the ST-type ones. The results obtained may be useful to scale up the fatigue behavior from small specimens to conventional ones, and to predict the fatigue behavior of bulk nanostructured materials.

Fractography

Figures 7 and 8 illustrate SEM images of the fatigue fracture surfaces of CG Ti-6Al-4 V alloy for ST-type (Fig. 7(a)) and SS-type (Fig. 8(a)) specimens, respectively. The area of fatigue crack initiation (Stage I), known as short crack growth propagation [30], is located on the surface of the specimen for ST-type specimens and extends into its depth for a distance ~ 50 μm (Fig. 7(b)). The reduction of the area of applied force is accompanied by an increase of the stress intensity factor K as a result of crack tip appearance, which leads to stress concentration on the tip. During consequent cyclic loading this stress results in the development of slip on the different planes and the formation of a stable crack growth region (Stage II). The surface ripples

("striations") can usually be found on the surface during Stage II (Fig. 6(c)). Such striations were observed on the ST-type fatigue fracture surface (Fig. 7(d)). The average width of these striations was about 0.3 μm. As reported in [31, 32], the most widely accepted mechanism for their formation is the consecutive closing and opening of the crack tip during cyclic loading. Stage III is represented by unstable growth. Fraction surface formation is dictated by static modes of failure. The ductile fracture surface, characterised by spherical dimples (Fig. 7(e)), was observed on the ST-specimens fracture surface. The size of the dimples is in the range 1~3 μm.

Same stages of the fatigue crack initiation and consequent propagation were observed on the fracture surface of the SS-type specimen of the same CG Ti-6Al-4 V alloy (Fig. 8(a)). The Stage I area is also located on the surface of the sample and its size is the same as for ST-type specimens: ~ 50 μm (Fig. 8(b)). The Stage II surface relief (Fig. 8(c)) has the same structure when compared with the ST-type. Only a difference in striation width (250–300 nm) was observed (Fig. 8(d)). A

Fig. 7 SEM images of the fatigue fracture surface of the CG hot rolled Ti-6Al-4 V alloy represented by ST-type specimen and tested under stress amplitude of 600 MPa to 9×10^4 cycles. (**a**) – close-up view of the fracture surface with indicated crack growth regions related to crack initiation (Stage I), stable crack growth (Stage II) and static failure (Stage III); (**b**) - fatigue fracture surface in the crack initiation region (Stage I); (**c**) - fatigue fracture surface in the stable crack growth region (Stage II); (**d**) - surface ripples observed in the stable crack growth region; (**e**) – fatigue fracture surface in the static failure region (Stage III). Arrows – crack growth direction
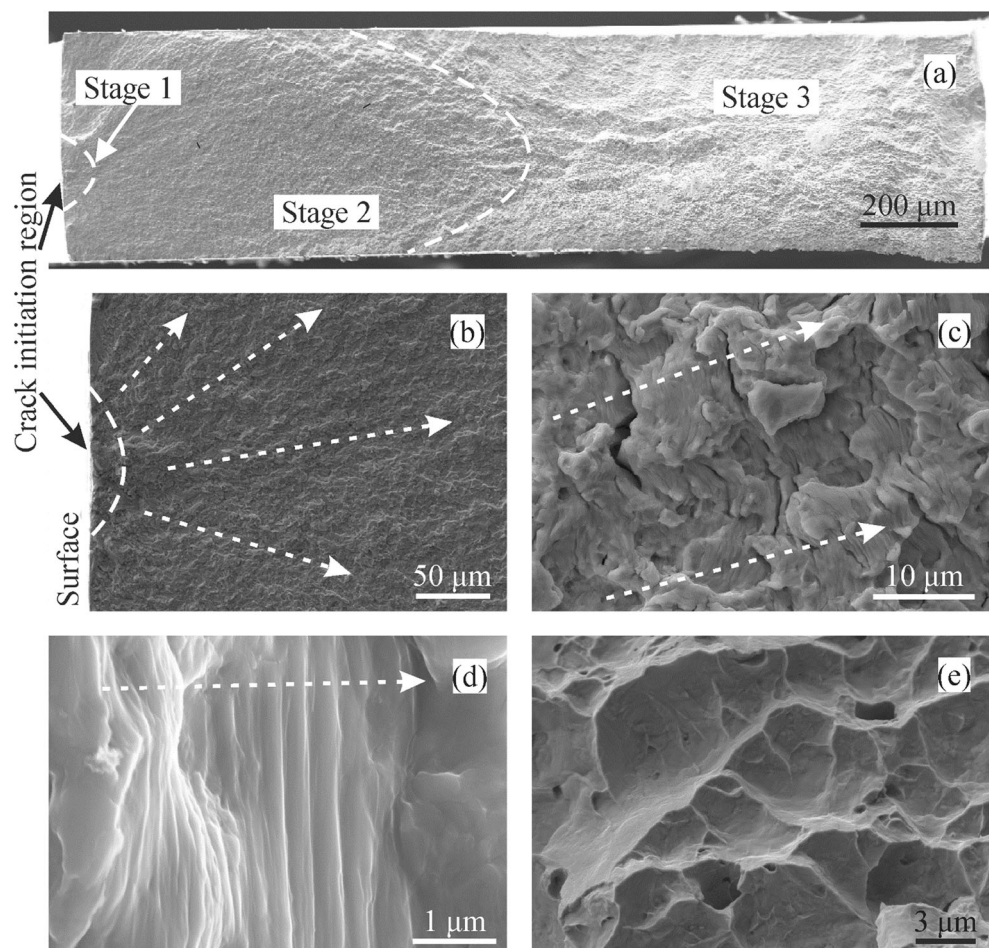
Fig. 8 SEM images of the fatigue fracture surface of the CG hot rolled Ti-6Al-4 V alloy for SS-type specimen tested under stress amplitude of 325 MPa to 1.2×10^5 cycles. (**a**) – close-up view of the fracture surface with indicated crack growth regions related to crack initiation (Stage I), stable crack growth (Stage II) and static failure (Stage III); (**b**) - fatigue fracture surface in the crack initiation region (Stage I); (**c**) - fatigue fracture surface in the stable crack growth region (Stage II); (**d**)- surface ripples observed in the stable crack growth region; (**e**) – fatigue fracture surface in the static failure region (Stage III). Arrows – crack growth direction
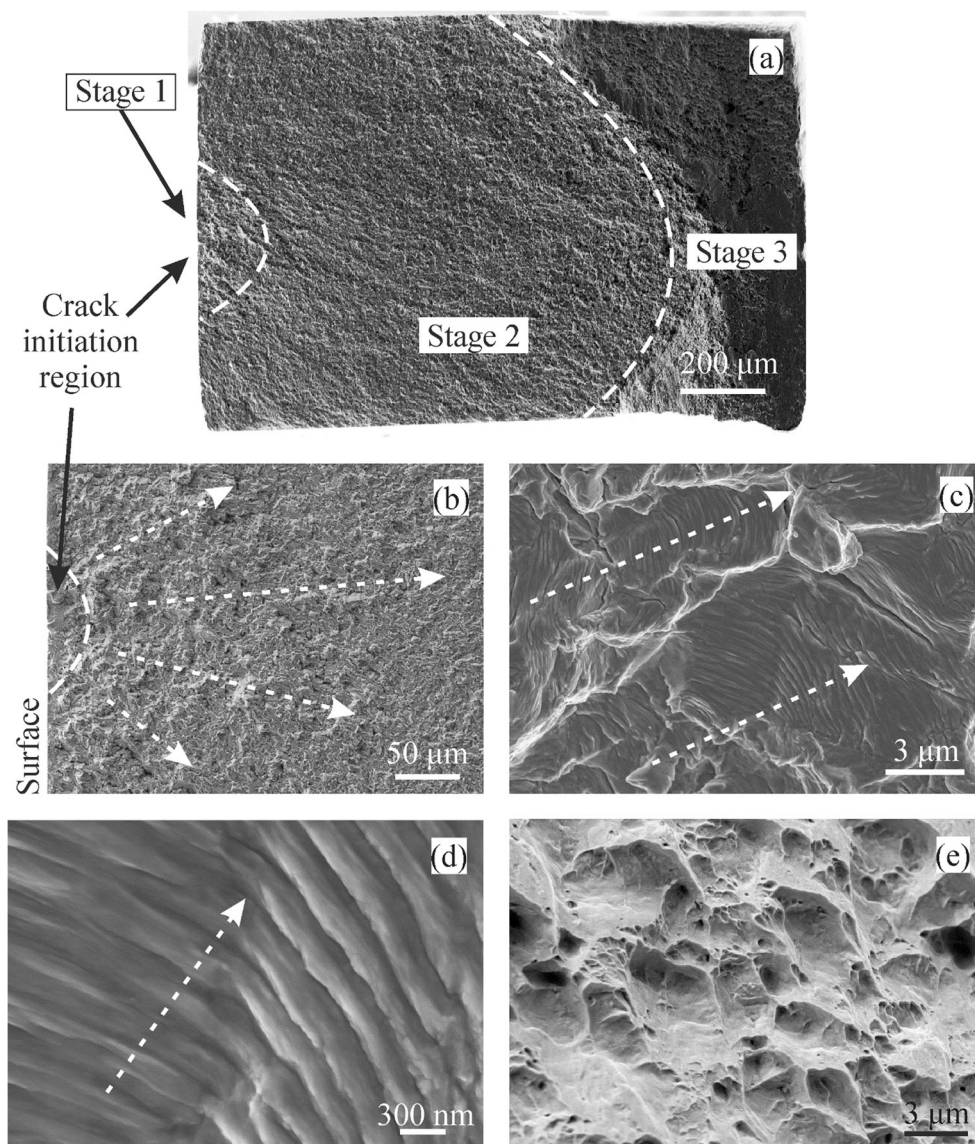
static failure area (Stage III) is also characterised by ductile fracture spherical dimples with size 1~3 μm (Fig. 8(e)).

Discussion

A significant difference in the tensile and fatigue behavior of SS and ST specimens is clearly observed. A lower elongation to failure value for ST samples can be explained by the fact that SS specimens have a smaller gauge length and surface area than the ST ones. Comparison of fatigue fracture surfaces for SS and ST specimens shows no significant difference in crack initiation and propagation properties. Therefore, there is no effect of sample geometry on fatigue and fracture mechanisms. However, a significant difference is seen in the Wohler's curves for the SS and ST samples. This difference is very significant in the HCF region, and less so in the LCF region (Fig. 6). It is known that fatigue crack initiation processes dictate fatigue life in the HCF region, so the crack initiation starts at a lower cycle number for SS samples than for ST ones. Despite this, surface roughness, due to defects introduced by polishing with the final 50 nm suspension, is lower than recommended by ASTM (Ra = 0.2 μm); a relation value between surface area and defect size is lower in the case of SS specimens. This can explain the significant difference in fatigue life observed in the HCF region (Fig. 6). On the other hand, good agreement of the obtained S-N curves in the LCF region was observed (Fig. 6). A fatigue life limit during cycling at high stress is driven by crack propagation processes. A fractography analysis showed that fracture kinetics remain the same during all stages of crack growth. Moreover, a microstructural aspect of the stable crack growth showed the same striation length for both specimen types (Figs. 7(d) and 8(d)). One can conclude that fatigue specimen roughness can affect

the fatigue behavior during HCF testing, and the scale factor for small specimens should be taken into account.

Conclusions

1. An original experimental technique for tensile and fatigue testing of sub-sized specimens was designed. The proposed technique is suitable for characterisation of HPT processed materials. Microstructural features of the materials, and stress concentration aspects, were taken into account during design of the testing tools.

2. A FEM analysis of the designed specimen-grip system reveals stress concentrators, which can misrepresent the experimental fatigue data. The obtained results aided modification of experimental equipment for mechanical testing to avoid undesirable data distortion.

3. The stress – strain curves for both standard size samples and sub-sized samples were plotted. A mechanical testing of sub-sized samples was conducted using an original in-house designed experimental technique. A comparison of mechanical properties for two different types of specimen geometry showed differences in elongation to failure values caused by differences in gauge length of the specimens.

4. The S – N curves on cyclic tension with $R = 0$ and constant load amplitude were measured for both types of specimen geometry. The data obtained showed a higher fatigue limit (550 MPa) for the standard specimens than for the sub-sized ones (350 MPa). This can be explained by the difference in the ratio of surface area to defect size for different specimen types. It leads to higher probability of crack initiation in the sub-sized specimens during high cycle fatigue testing.

5. An analysis of fatigue fracture surfaces reveals identical fatigue crack initiation and growth behavior for both specimen types. During high cycle fatigue testing, surface quality seems to be the main factor that can affect fatigue life limit during cyclic testing of sub-sized specimens.

6. The obtained results showed that sub-sized specimens could be potentially used to estimate the fatigue life of nanostructured materials, when only a small amount of material is available for analysis. However, as the fatigue life of such sub-sized specimens is underestimated, a scale factor could be introduced when estimating the fatigue of the standard specimens.

References

1. Legros M, Elliott BR, Rittner MN, Weertman JR, Hemker KJ (2000) Microsample tensile testing of nanocrystalline metals. Philos Mag A 80:1017–1026

2. Murase Y, Nagakawa J, Yamamoto N (2002) In-beam fatigue response of a low activation ferritic steel at 60°C. In: Sokolov MA, Lamdes JD, Lucas GE (eds) Small specimen test techniques: fourth volume. ASTM International, West Conshohoken

3. Meimei L, Stubbins LF (2002) Subsize specimens for fatigue crack growth rate testing of metallic materials. Small specimen test techniques: fourth volume. In: Sokolov MA, Lamdes JD, Lucas GE (eds) ASTM STP. ASTM International, West Conshohoken

4. Sriharsha HK, Pandey RK, Chatterjee S (1999) Towards standartising a sub-size specimen for fatigue crack propagation behavior of a nuclear pressure vessel steel. Eng Fract Mech 64:607–624

5. Farrell K, Sang Byun T, Wade Jones J, Gibson LT, Sitterson RG, Hashimoto N, Bailey JL, Gardner MJ (2002) Small specimen procedures for determination of deformation maps. Small specimen test techniques: fourth volume. In: Sokolov MA, Lamdes JD, Lucas GE (eds) ASTM STP. ASTM International, West Conshohoken

6. Valiev RZ, Zhilyaev AP, Langdon TG (2014) Bulk nanostructured materials: fundamentals and applications. Wiley, Hoboken

7. Valiev RZ, Islamgaliev RK, Alexandrov IV (2000) Bulk nanostructured materials from severe plastic deformation. Prog Mater Sci 45:103–189

8. Lyakishev NP, Alymov MI, Dobatkin SV (2003) Structural bulk nanomaterials. Russ Metall 3:191–202

9. Valiev RZ, Estrin Y, Horita Z, Langdon TG, Zehetbauer MJ, Zhu YT (2016) Fundamentals of superior properties in bulk nanoSPD materials. Mater Res Lett 4:1–21

10. Zeipper L, Zehetbauer M, Mingler B, Schafler E, Korb G, Karnthaler HP (2004) Mechanical properties of severely plastically deformed titanium. in Nanomaterials by severe plastic deformation. Zehetbauer M, Valiev RZ (eds) Wiley-VCH Verlag GmbH & co. KGaA, Weinheim

11. Sabirov I, Murashkin MY, Valiev RZ (2013) Nanostructured aluminium alloys produced by severe plastic deformation: new horizons in development. Mat Sci Eng A 560:1–24

12. Hokka M, Kokkonen J, Seidt J, Matrka T, Gilat A, Kuokkala V-T (2012) High strain rate torsion properties of ultrafine-grained aluminum. Exp Mech 52:195

13. Krasilnikov NA, Pakiela Z, Lojkowski W, Valiev RZ (2003) Grain refinement and mechanical properties of nickel subjected to severe plastic deformation. Solid State Phenom 94:51–54

14. Higuera-Cobos OF, Cabrera JM (2013) Mechanical, microstructural and electrical evolution of commercially pure copper processed by equal channel angular extrusion. Mater Sci Eng A 571:103–114

15. Wang CT, Gao N, Wood RJK, Langdon TG (2011) Wear behavior of an aluminum alloy processed by equal-channel angular pressing. J Mater Sci 46:123–130

16. Hug E, Prasath Babu R, Monnet I, Etienne A, Moisy F, Pralong V, Enikeev N, Abramova M, Sauvage X, Radiguet B (2017) Impact of the nanostructuration on the corrosion resistance and hardness of irradiated 316 austenitic stainless steels. Appl Surf Sci 392:1026–1035

17. Matykina E, Arrabal R, Valiev RZ, Molina-Aldareguia JM, Belov P, Sabirov I (2015) Electrochemical anisotropy of nanostructured titanium for biomedical implants. Electrochim Acta 176:1221–1232

18. Edalati K, Horita Z (2016) A review on high-pressure torsion (HPT) from 1935 to 1988. Mater Sci Eng A 652:325–352

19. Cheng X, Schroeder S, Berbon PB, Langdon TG (2010) Principles of ECAP–conform as a continuous process for achieving grain refinement: application to an aluminum alloy. Acta Mater 58: 1379–1386

20. Semenova IP, Yakushina EB, Nurgaleeva VV, Valiev RZ (2009) Nanostructing of Ti-alloys by SPD processing to achieve superior fatigue properties. Int J Mater Res 100:1691–1696

21. Semenova IP, Polyakov AV, Raab GI, Lowe TC, Valiev RZ (2012) Enhanced fatigue properties of ultrafine-grained Ti rods processed by ECAP-conform. J Mater Sci 47:7777–7781

22. Polyakov AV, Semenova IP, Huang Y, Valiev RZ (2014) Fatigue life and failure advanced characteristics of an ultrafine-grained Ti–6Al–4V alloy processed by ECAP and extrusion. Adv Eng Mater 16: 1038–1043

23. Yu E, Vinogradov A (2010) Fatigue behaviour of light alloys with ultrafine grain structure produced by severe plastic deformation: an overview. Int J Fatigue 32:898–907

24. Padilla HA II, Boyce BL (2010) A review of fatigue behavior in nanocrystalline metals. Exp Mech 50:5–23

25. Zhilyaev AP, Langdon TG (2008) Using high-pressure torsion for metal processing: fundamentals and applications. Prog Mater Sci 53:893–979

26. Valiev RZ, Langdon TG (2006) Principles of equal-channel angular pressing as a processing tool for grain refinement. Prog Mater Sci 51:881–981

27. Hohenwarter A, Bachmaier A, Gludovatz B, Scheriau S, Pippan R (2009) Technical parameters affecting grain refinement by high pressure torsion. Int J Mater Res 100:12

28. Pippan R, Scheriau S, Hohenwarter A, Hafok M (2008) Advantages and limitations of HPT: a review. Mater Sci Forum 584-586:16–21

29. Ruffing C, Kobler A, Courtois-Manara E, Prang R, Kübel C, Ivanisenko Y, Kerscher E (2015) Fatigue behavior of ultrafine-grained medium carbon steel with different carbide morphologies processed by high pressure torsion. Metals 5:891–909

30. Murashkin M, Sabirov I, Prosvirnin D, Ovid'ko I, Terentiev V, Valiev R, Dobatkin S (2015) Fatigue behavior of an ultrafine-grained Al-Mg-Si alloy processed by high-pressure torsion. Metals 5:578–590

31. Suresh S (1998) Fatigue of materials. Cambridge University Press, Cambridge

32. Milella PP (2013) Fatigue and corrosion in metals. Springer, Berlin